Dynamic interaction between discontinuity and noninvertibility: An analytical study

Shan Guan,[1] Bing-Hong Wang[2,3], Da-kai Wang,[4] and Da-Ren He[1,2,5,*]

[1] *Department of Physics, Northwestern University, Xian 710069, China*

[2] *China Center of Advanced Science and Technology (World Laboratory), P.O. Box 8730, Beijing 100080, China*

[3] *Department of Modern Physics, University of Science and Technology of China, Hefei 230026, China*

[4] *Department of Electronics, Northwestern University, Xian 710069, China*

[5] *Institute of Theoretical Physics, Academia Sinica, Beijing 100080, China*

(Received 28 April 1994; revised manuscript received 7 December 1994)

A discontinuous and noninvertible circle map is introduced to describe modulated relaxation oscillators. The boundaries of the parameter regions are calculated where images of the jumping gap completely cover the noninvertible region so that the dynamics of the system are abruptly changed. We show that a kind of structure called a "hole" may appear due to the interaction between these two competing characteristics and may lead to some dynamic features. The influence of the holes on the boundaries of Arnold tongues is also discussed.

PACS number(s): 05.45.+b

I. INTRODUCTION

Recently, one-dimensional maps, which are both discontinuous and noninvertible, have attracted much attention [1–16]. In such maps, one can observe types of transition behavior that are different from those of everywhere differentiable maps [3–7, 14, 15]. Nusse, Ott, and Yorke have discussed these transitions in generic cases and labeled them as "border-collision bifurcation" [18, 19].

In this paper we will give special attention to the circle maps, which describe relaxation oscillators in different fields, such as biology [8, 9, 13, 16], electronics [12, 15, 17], solid state physics [11], and other fields [10]. This kind of map often has two or more critical lines where discontinuity or noninvertibility occurs [9–12, 15]. Above these critical lines, the maps become both discontinuous and noninvertible, i.e., they have gaps and extrema. Recently, we suggested that in this kind of systems, the border-collision bifurcation may induce some type of intermittency. We have shown that the scaling behavior of average laminar lengths [20, 21], the distribution behavior of laminar lengths [22], the influence of external noise [23], and the scaling behavior of Lyapunov exponents [24] in this type of intermittency are different from those of the conventional three types. As far as we know, up to now, there have been three experimental proofs on this type (named type V) of intermittency [25–27]. In addition to the experimental observation of type-V intermittency in an electronic relaxation oscillator made by He and co-workers [25, 22, 23], Wunderlich, Moorman, and Koch have observed an intermittency with the logarithmic dependence on the control parameter. This is believed to be caused by a type-V intermittency in a gas discharge system [26]. Richter *et al.* have confirmed a type-V intermittency in the oscillations of P-type germanium [27]. We are convinced that the dynamic features induced by the interaction between discontinuity and noninvertibility can also appear in many practical systems and are of general interest.

In recent publications [14,15] we have discussed some dynamic behaviors other than type-V intermittency induced by the interactions between discontinuity and noninvertibility, such as the coexistence of attractors induced by holes and the disappearance of chaos due to a complete covering of the noninvertible region by gap images. In this paper we will discuss these behaviors further by using a piecewise linear circle map in order to do more analytical treatment. Also, we will discuss how the boundaries of Arnold tongues depend on this interaction. The paper is organized as follows. We will introduce the system, calculate the Lyapunov exponent, and discuss the partitions of the parameter space in Sec. II. In Sec. III we will calculate the boundaries of the regions where the noninvertible region of the map is completely covered by the images of the gap, and will discuss the abrupt change of the system dynamics. In Sec. IV we will define the concept of hole, discuss the possible number of holes, and discuss the condition of their appearance. In Sec. V we will calculate the boundaries of Arnold tongues and the ranges where periodic attractors coexist and discuss the role of holes in these calculations. In Sec. VI we will share some further thoughts.

II. SYSTEM

The system we have extensively studied [12,15,21] is a circle map describing a thyratron electronic relaxation oscillator which was often used in electronic instruments before 1970. Today people use similar circuits but made of modern electronic parts [25,22,23]. The Poincaré map of the system and its corresponding integrate-and-

*Author to whom correspondence should be addressed at Department of Physics, Northwestern University, Xian 710069, China.

fire model, in which a variable relaxes between a sine-modulated upper threshold and a constant lower threshold, may also be thought of as a model of some biological systems [8,9] or some systems in solid state physics [12]. Numerical investigations, along with some analytical investigations, have been done. However, the analytical discussion is difficult due to the strong nonlinear character and the implicit function form of the map. In order to do more analytical calculations and get more quantitative understanding, we reduce this model into a simplified one, which can still preserve the main characteristics and dynamic features.

In the simplified model, a variable v relaxes linearly between a trapezoidal wave-modulated upper threshold and a constant lower threshold as shown in Fig. 1. The circle map describing it will be piecewise linear and thus very easy to analyze. According to the geometry shown in Fig. 1, the map is easily deduced as follows after performing some algebra. By taking the switching points of t at the lower threshold, namely, t_m, as the Poincaré section, the map will read

$$t_{m+1} = f_i(t_m) = k_i t_m + b_i \qquad (i = 1-4), \tag{1}$$

where

$$k_1 = \frac{I_i(dI_d + A)}{I_d(dI_i - A)},$$

$$b_1 = \frac{(dI_d + A)[d(1-A) - (n-d)A]}{dI_d(dI_i - A)} + \frac{d(1-A) - (n-d)A}{dI_d},$$

$$k_2 = 1, \qquad b_2 = J(1 + A),$$

$$k_3 = \frac{I_i(dI_d - A)}{I_d(dI_i + A)},$$

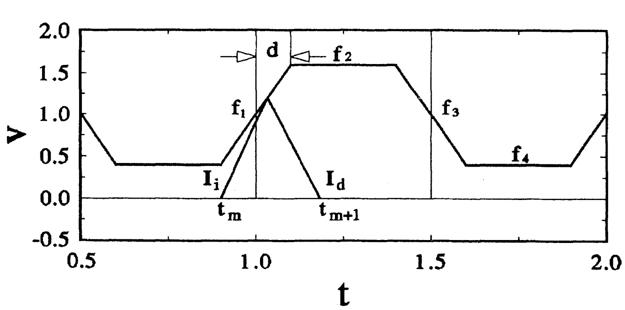

FIG. 1. A schematic drawing to show the integrate-and-fire model describing the trapezoidal wave-modulated relaxation oscillator.

$$b_3 = \frac{(dI_d - A)[d(1-A) + (n + 0.5 + d)A]}{dI_d(dI_i + A)} + \frac{d(1-A) + (n + 0.5 + d)A}{dI_d},$$

$$k_4 = 1, \qquad b_4 = J(1 - A).$$

The ranges of definition of the function branches are, for f_2, f_2, f_3, and f_4, respectively,

$$t_{mi} \le t_m < t_{mc},$$

$$t_{mi} = n - d - \frac{1-A}{I_i}, \qquad t_{mc} = n + d - \frac{1+A}{I_i};$$

$$t_{mc} \le t_m < t_{mm}, \qquad t_{mm} = n + 0.5 - d - \frac{1+A}{I_i};$$

$$t_{mm} \le t_m < t_{me}, \qquad t_{me} = n + 0.5 + d - \frac{1-A}{I_i};$$

$$t_{me} \le t_m < 1 + t_{mi}.$$

A is the amplitude of the trapezoidal wave, $4d$ is the difference between its lower side and upper side, I_i is the constant arising slope, I_d is the absolute value of the constant falling slope of the relaxation oscillation, and $J = \frac{1}{I_i} + \frac{1}{I_d}$.

This map has two critical lines. The discontinuity appears at $I_i = \frac{A}{d}$ and the noninvertibility appears at $I_d = \frac{A}{d}$. These two lines divide the parameter space $I_d - I_i$ into four regions of qualitatively different behaviors [9–12,15]. In the region where $I_i > \frac{A}{d}$ and $I_d > \frac{A}{d}$, the map is continuous as well as invertible. The attractors can be either quasiperiodic or periodic [28,10]. In the region where $I_i > \frac{A}{d}$ but $I_d < \frac{A}{d}$, the map is continuous but noninvertible. The attractors can be chaotic or periodic [28–30, 1]. In the region where $I_i < \frac{A}{d}$ but $I_d > \frac{A}{d}$, the map is discontinuous but invertible and the attractors can only be periodic [1, 31]. In the region where $I_i < \frac{A}{d}$ and $I_d < \frac{A}{d}$, the map becomes both discontinuous and noninvertible. This is the region in which we are interested. In this region, the f_1 branch of the mapping function (1) does not exist. The dynamics of the system can be described by a map composed of three linear function branches. If we let $d \to 0$, we obtain an integrate-and-fire model, in which the variable v relaxes between a rectangular wave-modulated upper threshold and a constant lower threshold as shown in Fig. 2. It shows, qualitatively, the exact same dynamic behavior as map (1) does in the supercritical region where $I_i < \frac{A}{d}$ and $I_d < \frac{A}{d}$. Here the mapping function is much more simple, hence the calculation will be much easier.

With a method similar to what we used for map (1), we have obtained this mapping as follows:

$$t_{m+1} = f_i(t_m) = k_i t_m + b_i \qquad (i = 1-3), \tag{2}$$

where

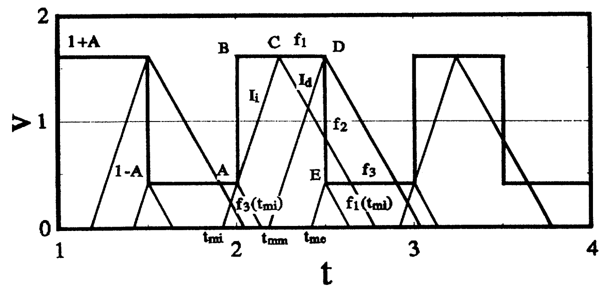

FIG. 2. Schematic drawing to show the integrate-and-fire model describing the rectangular wave-modulated relaxation oscillator. This figure also shows a complete covering situation, which will be explained in Sec. III.

$$k_1 = 1, \qquad b_1 = J(1 + A),$$

$$k_2 = -\frac{I_i}{I_d}, \qquad b_2 = \left(1 + \frac{I_i}{I_d}\right)(n + 0.5),$$

$$k_3 = 1, \qquad b_3 = J(1 - A).$$

The ranges of definition of the three function branches are, for f_1, f_2, and f_3 respectively,

$$t_{mi} \leq t_m < t_{mm}, \quad t_{mi} = n - \frac{1 - A}{I_i},$$

$$t_{mm} = n + 0.5 - \frac{1 + A}{I_i};$$

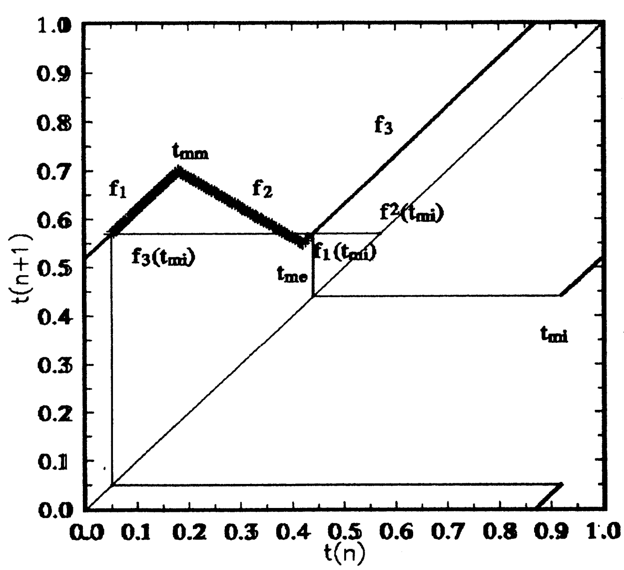

FIG. 3. Mapping function of (2) with the parameters $A = 0.6$, $I_i = 5.0$, and $I_d = 8.0$. The region covered by the images of the gap G is indicated by crosses.

$$t_{mm} \leq t_m < t_{me}, \quad t_{me} = n + 0.5 - \frac{1 - A}{I_i};$$

$$t_{me} \leq t_m < 1 + t_{mi}.$$

A is the amplitude of the rectangular wave, I_i is the constant arising slope, I_d is the absolute value of the constant falling slope of the relaxation oscillation, and $J = \frac{1}{I_i} + \frac{1}{I_d}$. This map does not have the above-mentioned type of critical lines. For any finite values of I_i and I_d, the map is both discontinuous and noninvertible. From now until Sec. V, we will discuss only map (2).

Considering that two branches of map (2) have slope 1, we can get an expression of the Lyapunov exponents easily. If we assume that in an iteration trajectory of map (2) there are Q times of iterations visiting $[t_{mi}, t_{mm})$, P times visiting $[t_{mm}, t_{me})$, and W times visiting $[t_{me}, 1 + t_{mi})$, the Lyapunov exponent λ can be calculated as

$$\begin{aligned}\lambda &= \lim_{N\to\infty}\left[\frac{1}{N}\sum_{j=0}^{N-1}\ln|f'(t_{mj})|\right] \qquad (N = Q + P + W)\\ &= \lim_{N\to\infty}\left[\frac{1}{N}\left(\sum_{j=1}^{Q}\ln|1| + \sum_{j=1}^{P}\ln|1 - I_iJ|\right.\right.\\ &\qquad\left.\left. + \sum_{j=1}^{W}\ln|1|\right)\right]\\ &= \lim_{N\to\infty}\left[\frac{1}{N}\sum_{j=1}^{P}\ln\left|\frac{I_i}{I_d}\right|\right]\\ &= \lim_{N\to\infty}\left[\frac{P}{N}\ln\left|\frac{I_i}{I_d}\right|\right]. \end{aligned} \tag{3}$$

Clearly, the sign of the Lyapunov exponent of a trajectory only depends on the absolute value of the slope of the f_2 branch. We thus call it the "characteristic branch." When P is not zero, $I_i > I_d$ and the absolute value of the slope is larger than 1, $\lambda > 0$, and the system shows only chaotic motion; when $I_i < I_d$, the absolute value of the slope is smaller than 1, $\lambda < 0$, and the system shows only periodic motion. This means that the diagonal divides the I_i-I_d parameter plane in two parts with different dynamical behaviors. If $P = 0$, i.e., the iterations do not visit the characteristic branch, the Lyapunov exponent can only be zero. That gives rise to some special regions in the parameter plane where quasiperiodic or periodic motion with marginal stability may occur.

III. BOUNDARIES OF THE REGIONS COVERED BY GAP IMAGES

Figure 3 shows a typical mapping function $f(t_m)$ (mod1), of (2), which is obviously discontinuous and noninvertible. Because $f_2(t_{mm}) - f_3(t_{me}) = \frac{2A}{I_d} > 0$, one can always see a maximum at t_{mm} and a minimum at t_{me}.

They give rise to an overlapping (or noninvertible) region on the $f(t)$ axis, where three overlapping branches of the mapping function are positioned. We indicate the region by $O = [f_3(t_{me}), f_1(t_{mm})]$. When $I_i < 4A$, t_{mm} merges with t_{mi} and the f_1 branch disappears. In this case we should define O as $O = [f_3(t_{me}), f_2(t_{mi})]$. There are only two overlapping branches. Also, the gap at t_{mi} gives rise to a forbidden region $G = [f_3(t_{mi}), f_1(t_{mi})]$ on the $f(t)$ axis. When $J > \frac{1}{4A}$, in a return map (mod1), $f_3(t_{me})$ will be lower than $f_1(t_{mi})$, as shown in Fig. 4. In some cases, $f_3(t_{me})$ is even lower than $f_3(t_{mi})$. Thus in such a return map as shown in Fig. 4, one can see a forbidden region smaller than G or not see any forbidden region at all. However, please note that in Fig. 2 the region of the upper threshold between A and C is never reached by iterations. Therefore, roughly speaking, the region $G = [f_3(t_{mi}), f_1(t_{mi})]$ and all of its forward images form the well-known "transient region" where only transient iterations can visit. We then say that the forbidden region exists implicitly in the case when $J > \frac{1}{4A}$. If we choose t_m and t_{m+1}, the times when the relaxation oscillations reach the upper threshold, as the Poincaré section, the forbidden region will always exist explicitly.

In the type of circle maps we are discussing, the transient region often "completely covers" the noninvertible region. That means it covers two of the three overlapping mapping branches here. The map then becomes invertible but discontinuous if the transience is ignored. In some of the systems, in all of the supercritical region, the noninvertibility is completely covered by gap images. As we know, the first example for complete covering is an integrate-and-fire model in which a variable relaxes between a triangular wave-modulated upper threshold and a constant lower threshold [32]. The second one is a model in which both the thresholds are modulated by synchronizing signals with the exact same form and the resetting time is zero [33]. We are presently working on the third example, which is an integrate-and-fire model with "current modulation" [34, 31]. In a general system, such as in the current system, only part of the supercritical region is covered [12,15]. It is interesting that the complete covering may serve as a way to eliminate chaos if the Poincaré map of a system is both discontinuous and noninvertible and the size, as well as the position of the discontinuity, can be controlled.

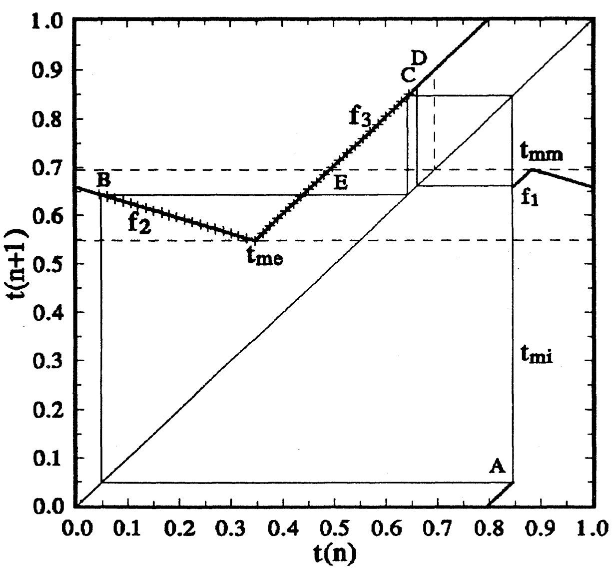

FIG. 4. Mapping function of (2) with the parameters $A = 0.6$, $I_i = 2.6$, and $I_d = 8.2$. The region covered by the images of the gap G is indicated by crosses. The overlapping region O is indicated by dashed lines. The stable period-three orbit ABC is computed with a fixed initial value $t_0 = 0.846$. The first 200 iterations were ignored to avoid the transience and then 500 were recorded.

Now we calculate the boundaries of the completely covered regions in map (2). The set of G and its images is

$$S = \lim_{n\to\infty} \bigcup_{i=1}^{n} f^i(G). \tag{4}$$

If set S only covers part of region O, as the segments $[B, t_{me}]$ and $[t_{me}, E]$ in Fig. 4, the iterations from the rest of region O (as the part of f_2 branch between t_{mm} and B in Fig. 4), i.e., the difference between O and the intersection of S and O,

$$D_1 = O \setminus (S \bigcap O), \tag{5}$$

may reach region S. As shown in Fig. 4, A, B, C are a stable period-three orbit with the parameters chosen, B is just inside D_1, and its image C is inside the first image of G (indicated by crosses). Therefore, the transient region, which is forbidden for iteration when the transience is ignored, is

$$S_h = S \setminus (D \bigcap S), \tag{6}$$

where D is defined as

$$D = \lim_{n\to\infty} \bigcup_{i=1}^{n} f^i(D_1). \tag{7}$$

In map (2), if S covers all of the characteristic region $[t_{mm}, t_{me})$, we can prove that it should also cover two of the three overlapping branches in O. We can also prove that $S = G + f(G)$. The reason is that in this case the image of $f_3(t_{mi})$ will certainly fall on the f_1 branch and the image of $f_1(t_{mi})$ will certainly fall on f_3 branch, as shown in Fig. 3. Then it is easy to obtain

$$f_1(f_3(t_{mi})) = t_{mi} + 2J, \tag{8}$$

$$f_3(f_1(t_{mi})) = t_{mi} + 2J\ . \tag{9}$$

In this situation, the positions of the further iterations of both ends of G are the same. The size of the rest of the images of G is zero, as shown in Fig. 3. Figure 3 also shows that G and its first image $S = G + f(G)$ completely cover the noninvertible region. However, as discussed above, S is not the transient region S_h yet. In order to calculate the boundary of the region where $P = 0$, we have to consider the part of overlapping region that is not covered by S. We must also prevent the iterations from this part from entering into the characteristic region in the next period of the driving signal. In this calculation, we only discuss the situation $I_i > 4A$. The discussion for $I_i < 4A$ is similar and thus is ignored.

Referring to Fig. 2, we consider that the first image of G should cover the characteristic region $[t_{mm}, t_{me})$. That gives us

$$f_3(t_{mi}) < t_{mm}, \tag{10}$$

$$f_1(t_{mi}) > t_{me}. \tag{11}$$

In Fig. 2 the overlapping region is $[f_3(t_{me}), f_1(t_{mm})]$. Therefore, according to the definition of the transient region, we should prevent the iterations from this part from entering into the characteristic region in the next period of the driving signal. Thus we have

$$f_1(t_{mm}) < 1 + t_{mm} \tag{12}$$

or

$$f_3(t_{me}) < 1 + t_{me}. \tag{13}$$

The completely covered region will satisfy (10), (11), and (12), or (10), (11), and (13).

When I_d is small, the falling branch of the relaxation oscillation may cross many periods of the driven rectangular wave. We have to use two integers N and N' to describe this situation. Assume that I_d satisfies the condition

$$\frac{2A}{N+1-\frac{2A}{I_i}} < I_d < \frac{2A}{N-\frac{2A}{I_i}}, \tag{14}$$

which means that the length of region G, $\mid G \mid = 2AJ$, satisfies $N <\mid G \mid< N+1$. At the same time, assume that I_d also satisfies

$$\frac{1-A}{N'+1} < I_d < \frac{1-A}{N'}, \tag{15}$$

which means that the length $\mid f_3(t_{mi}) - t(A) \mid$ satisfies $N' <\mid f_3(t_{mi}) - t(A) \mid< N'+1$. Here $t(A)$ means the time of point A in Fig. 2. Now we can understand that Fig. 2 shows $N = 1$ and $N' = 1$. In a general case, with a similar consideration, we have

$$f_3(t_{mi}) < N' + t_{mm} \tag{16}$$

and

$$f_1(t_{mi}) > N + N' + t_{me}, \tag{17}$$

$$f_1(t_{mm}) < N + N' + 1 + t_{mm}, \tag{18}$$

or

$$f_3(t_{me}) > N' + t_{me}. \tag{19}$$

However, considering the definition of N', (15), and that $f_3(t_{mi}) - t(A) = f_3(t_{me}) - t(E)$, (19) is always satisfied. The general condition of the boundaries of the completely covered regions will thus be determined only by (14)–(18). Similarly, the inequality (13) can be ignored when $N = 1$ and $N' = 1$.

Solving (16)–(18), we get

$$\frac{1-A}{N'+\frac{1}{2}-\frac{1+A}{I_i}} < I_d, \tag{20}$$

$$\frac{1+A}{1+N+N'-\frac{1+A}{I_i}} < I_d < \frac{1+A}{\frac{1}{2}+N+N'-\frac{1+A}{I_i}}. \tag{21}$$

Combining (20), (21), (14), and (15), we get

$$M_1 < I_d < M_2, \tag{22}$$

where

$$M_1 = \max\left(\frac{2A}{N+1-\frac{2A}{I_i}}, \frac{1-A}{N'+1}, \frac{1-A}{N'+\frac{1}{2}-\frac{1+A}{I_i}}, \frac{1+A}{1+N+N'-\frac{1+A}{I_i}}\right),$$

$$M_2 = \min\left(\frac{2A}{N-\frac{2A}{I_i}}, \frac{1-A}{N'}, \frac{1+A}{\frac{1}{2}+N+N'-\frac{1+A}{I_i}}\right).$$

The general condition of the boundaries of completely covered regions will be determined by (22).

Using (22) with a fixed value $A = 0.6$, we have drawn the completely covered regions in Fig. 5, where they are indicated by dense black lines. One can see that these regions are separated from each other and are becoming narrower and narrower as I_d decreases. In order to see the details where I_d is small and to compare the analytical results expressed by (22) with the numerical results, we have computed the Lyapunov exponent in the range $0 < I_d < 0.4$ with the fixed values $A = 0.6$ and $I_i = 5.0$. The results are shown in Fig. 6. We can see many horizontal plateaus, where $\lambda = 0$, in the figure. They should be completely covered regions. In order to compare them with (22), we have proved that (22) can be simplified only into (21) when $A > \frac{1}{\sqrt{3}}$ and $I_i > 2(1+A)$. Specifically,

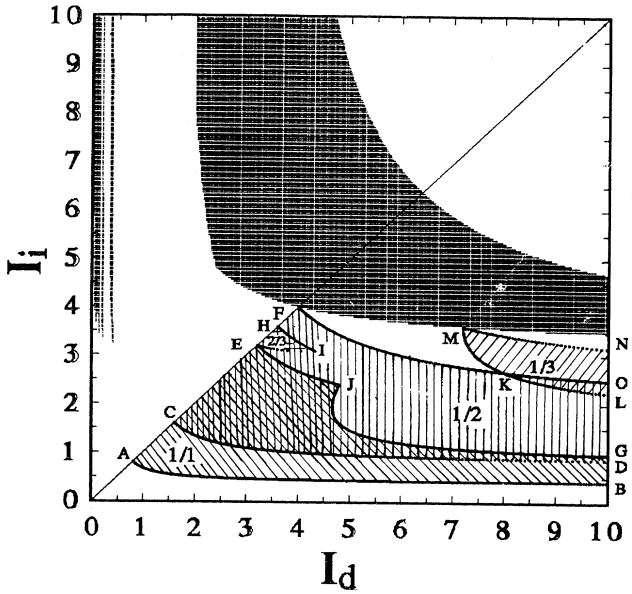

FIG. 5. A parameter plane I_i-I_d with $A = 0.6$. The region indicated by dense black lines is completely covered and drawn by the conditions (22). The region $ABGJE$ is the phase-locked region with the rotation number $W = \frac{1}{1}$, the region $CDOF$ is that with $W = \frac{1}{2}$, the region MLN is that with $W = \frac{1}{3}$, and the region EIH is that with $W = \frac{2}{3}$. The analytical calculation of the phase-locked regions will be presented in Sec. V.

when $I_i = 5.0$ and $A = 0.6$, we get $N = 3N'$ and thus (21) becomes

$$\frac{0.4}{N' + 0.17} < I_d < \frac{0.4}{N' + 0.045}. \tag{23}$$

In Fig. 6 the results of (23) are indicated by the wide horizontal lines beneath the plateaus and show very good consistency.

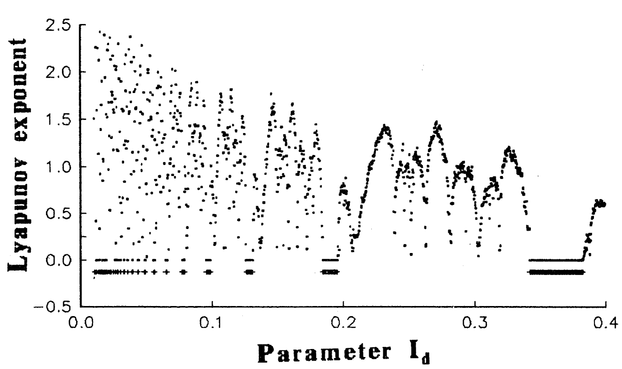

FIG. 6. Lyapunov exponent spectrum computed by map (2). The wide horizontal lines beneath the spectrum indicate the analytical results by (23) for comparison. The parameters are $A = 0.6$, $I_i = 5.0$, and $t_0 = 0.5$ and the first 200 iterations were ignored to avoid the transience.

We now define the rotation number of a trajectory in the current system in order to discuss the condition of the appearance of quasiperiodic or periodic motion in the completely covered regions. One of us (D.-R.H.) and his co-workers have proposed [12] a "firing number" to denote how many oscillations there are, on average, in one period of the driving signal T when discussing our original nonlinear system. It is defined as

$$F = \lim_{n\to\infty} \frac{Tn}{f^n(t_0) - t_0}. \tag{24}$$

The rotation number can be defined as $W = \frac{1}{F}$. Because T is fixed and equals 1 in the current system, W can be expressed as

$$W = \lim_{n\to\infty} \frac{f^n(t_0) - t_0}{n}. \tag{25}$$

When an iteration trajectory is periodic, it satisfies $f^P(t) = Q + t$, where P and Q are integers. The rotation number becomes $W = \frac{Q}{P}$ in this case. If the characteristic region $[t_{mm}, t_{me})$ is covered by S_h so that iterations cannot visit it if the transience is ignored, we have $\lambda = 0$. The rotation number can be expressed as

$$W = \lim_{n\to\infty} \frac{J[n + A(V - U)]}{n}, \tag{26}$$

where V is the number of visits by iterations to the f_1 branch, U is the number of visits to f_3 branch, and $n = V + U$. When W is a rational number, the motion should be periodic with marginal stability. Otherwise, W is irrational and the motion should be quasiperiodic. Numerically we have observed the abrupt transition from a chaotic motion (in the region where $I_i > I_d$) or a periodic motion (in the region where $I_i < I_d$) to a quasiperiodic motion when changing a control parameter to cross the boundary of a completely covered region. This transition, having been observed also in a biological system [16] and in other systems of this type [34], should have different characteristics.

IV. HOLE AND ITS APPEARANCE CONDITION

When studying a period-p attractor of the map, including its evolution and loss of stability, one has to consider the discontinuous (or jumping) behavior of $f^p(t)$ at some inverted images of t_{mi}, i.e., $f^{-k}(t_{mi})$ $(k < P)$. These discontinuities are only implicitly expressed in the $f(t)$ mapping functions as can be seen in Fig. 3 or 4, but will be explicitly expressed in the $f^p(t)$ mapping function. If the number k of the inverted images falls into the noninvertible region O there will be two or three $f^{-k}(t_{mi})$, denoted by $f_i^{-k}(t_{mi})$ $(i = 1$–$3)$, around either the maximum or the minimum. Here i indicates that it is on the f_i branch. We define the region $(f_1^{-k}(t_{mi}), f_2^{-k}(t_{mi}))$ or $(f_2^{-k}(t_{mi}), f_3^{-k}(t_{mi}))$ as the hole if i can take values of only 1–2 or 2–3. When i=1–3, we define one of these two regions, the one smaller in size, as the "hole". Please note that this definition suits the original form (1) and (2) of mapping and does not necessarily suit what is shown in a return map (mod 1) such as Fig. 3 or 4. By using p-fold iterated mapping, one can show that the hole is really a kind of structure as described by its name and that the appearance of the hole is a kind of critical phenomenon. As an example, Fig. 7(a) shows a situation where the minimum t_{me} is higher than t_{mi} so that $f^{-1}(t_{mi})$ cannot fall in region O and thus is single valued. Therefore, if we need to study a period-two attractor, the corresponding two-fold iterated mapping function in Fig. 7(b) shows

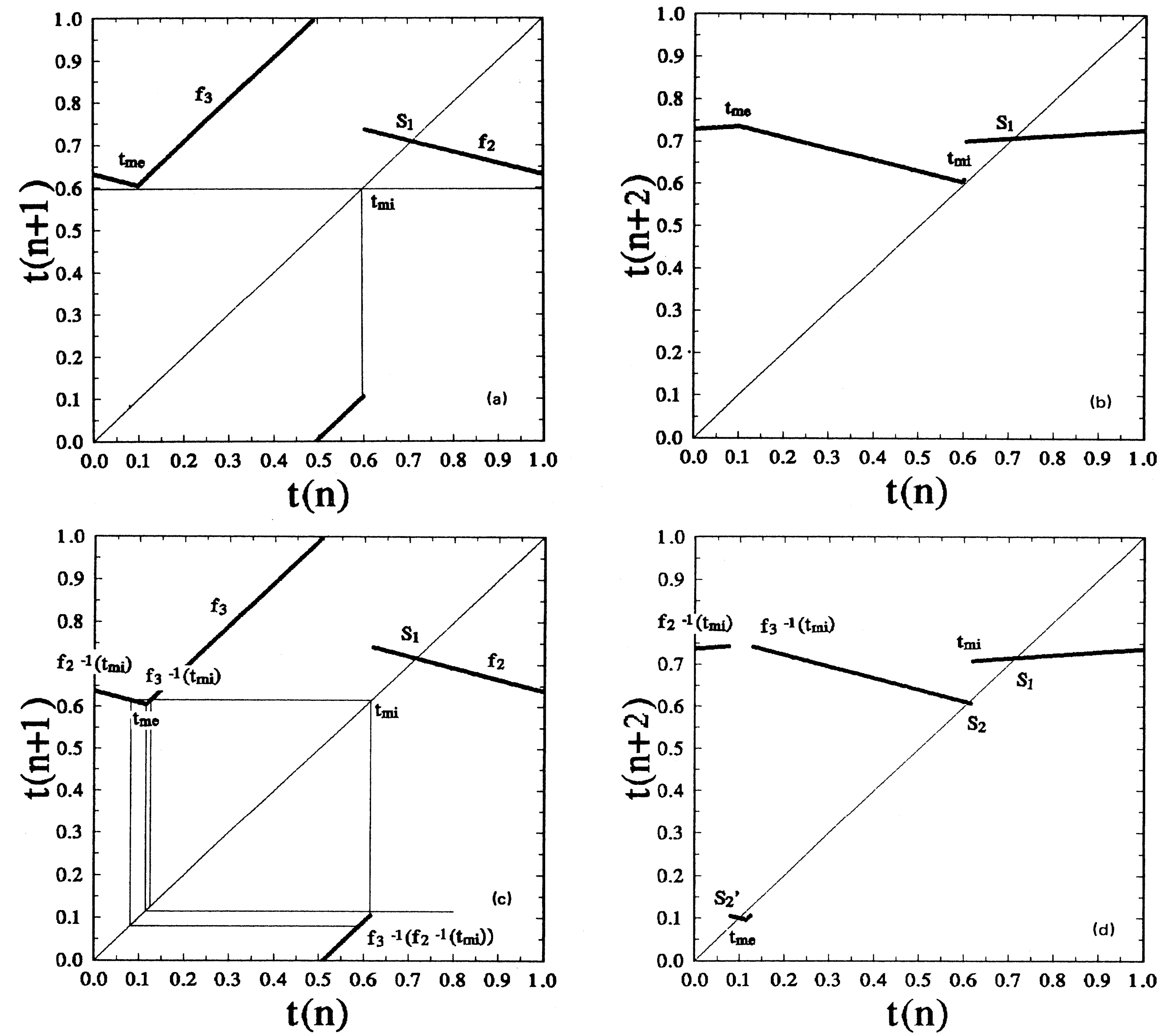

FIG. 7. (a) Mapping functions of (2) (mod 1) computed at $I_i = 1.0$, $I_d = 3.8$, and $A = 0.6$ (position P_1 in Fig. 8). The thin solid lines show the position of discontinuity t_{mi}, which is still lower than the minimum t_{me}. The basin of the only attractor S_1 is the whole phase space. (b) Two-fold iterated mapping function of (2) (mod 1) computed with the same parameter values as in (a). There is no hole yet and S_1 is the only attractor. (c) Mapping function of (2) (mod 1) computed at $I_i = 1.04$, $I_d = 3.8$, and A=0.6 (position P_2 in Fig. 8). The thin solid lines show the position of t_{mi}, its first inverted image $f_2^{-1}(t_{mi})$ and $f_3^{-1}(t_{mi})$, its second inverted image $f_3^{-1}(f_2^{-1}(t_{mi}))$, and the minimum t_{me} and its first inverted image (falling in the forbidden region). (d) Two-fold iterated mapping function of (2) (mod 1). The parameter values are the same as in (c). It is shown that there is a hole between $f_2^{-1}(t_{mi})$ and $f_3^{-1}(t_{mi})$ and that a stable period-two orbit S_2 and S_2' appears, the basin of attraction of which is the hole and its first backward iteration [see (c)]. At the same time the original period-one attractor S_1 is still stable and attracts the iterations from the rest of the phase space.

that no hole appeared. When a parameter, for example I_i, is increased so that t_{mi} becomes larger than t_{me}, $f^{-1}(t_{mi})$ falls in O and thus is multivalued, as shown by Fig. 7(c). Thus, in the two-fold map, the piece of the mapping function between $f_2^{-1}(t_{mi})$ and $f_3^{-1}(t_{mi})$ is cut off by the sudden appearance of the pair of discontinuities to form a real hole, as shown in Fig. 7(d).

If all the further inverted images of $f^{-k}(t_{mi})$ and t_*, i.e., $f_i^{-j}(t_{mi})$ $(k < j < p)$ and $f^{-s}(t_*)$ $(1 < s < p-k-1)$, do not fall in G (t_* denotes either t_{mm} or t_{me}), the pairs of discontinuities at all the $f_i^{-j}(t_{mi})$ $(k < j < p)$ around the extrema $f^{-s}(t_*)$ $(1 < s < p-k-1)$ in the p-fold iteration mapping will also form holes. Thus all of the holes together will equal $p-k$. We call these $p-k$ holes a "set of holes" since all of them are formed by the backward iterations of $f^{-k}(t_{mi})$. If any $f_i^{-j}(t_{mi})$ $(k < j < p)$ (i=1–3) in this set falls in region O again, $f_i^{-j}(t_{mi})$ will be multivalued. We shall have to trace the inverted images of all of the $f_i^{-j}(t_{mi})$ to count holes according to the same rule. Therefore, if all the inverted images of the jth generation fall in O, we may have to trace 3^j inverted images of the next generation. That makes difficulties for both the analytical and the numerical investigations when P is large enough. One may think, according to the above statements, that the number of holes may increase very fast when P increases and form an infinite set when $P \to \infty$. That may not be true because $f_i^{-j}(t_{mi})$ and $f^{-s}(t_*)$ often fall in G and stop the increase of the number of holes. We shall present a numerical investigation in Sec. VI to show the situation. For the current map (2), the condition of the appearance of so-called $(k+1)$-order holes can be expressed as

$$f(t_{me}) < f^{-k}(t_{mi}) < f(t_{mm}). \tag{27}$$

V. BOUNDARIES OF ARNOLD TONGUES AND REGIONS WHERE PERIODIC ATTRACTORS COEXIST

We have proved in Sec. II that the diagonal $I_i = I_d$ divides the parameter plane I_i-I_d in two regions where either periodic or chaotic attractors exist. Now we calculate the boundaries of Arnold tongues in the region where $I_d > I_i$.

As is known, the conditions of a period-p attractor are

$$f^p(t_{mj}) = Q + t_{mj}, \tag{28}$$

$$\prod_{j=1}^{P} | f'(t_{mj}) | < 1, \tag{29}$$

where $j = 1, 2, \ldots, p$ denotes the jth stable periodic point. For the current map there should be at least one t_{mj} on f_2 branch, i.e., in region $[t_{mm}, t_{me})$, to satisfy (29). We denote it as t_{2mj} and define function $g(t_{2mj})$ as

$$g(t_{2mj}) = f^{p-1}(f_2(t_{2mj})) - Q - t_{2mj}. \tag{30}$$

$g(t_{2mj})$ is continuous and differentiable in $[t_{mm}, t_{me})$ in a parameter region if either of the following conditions is satisfied. First, holes cannot appear here. This means there cannot be any $f_2^{-k}(t_{mi})$ $(k < p)$. Second, holes can exist, but the edge of the hole on f_2, $f_2^{-k}(t_{mi})$, never collides with any t_{2mj}. This means it is impossible to have $t_{2mj} = f_2^{-k}(t_{mi})$. In such a region, the boundary of the period-p Arnold tongue should be decided by

$$g(t_{2mj}) = 0, \tag{31}$$

$$t_{mm} < t_{2mj} < t_{me}. \tag{32}$$

While in a region where there are r values of t_{2mj} $(r < p)$ that satisfy $t_{2mj}(r) = f_2^{-k}(t_{mi})$, $g(t_{2mj})$ is discontinuous at $t_{2mj}(r)$. We then have to divide the region $[t_{mm}, t_{me})$ into $r+1$ subregions, i.e., S_i $(i = 1, 2, \ldots, r+1)$, so that in every one of them $g(t_{2mj})$ becomes differentiable. Thus the condition of the boundary of the period-p Arnold tongue becomes

$$g(t_{2mj}) = 0, \tag{33}$$

$$t_{2mj} \in S_i. \tag{34}$$

This means we have to discuss respectively each subregion because the jumping behavior of $g(t_{2mj})$ at the boundary of S_i may induce the jumping of the corresponding boundary of the periodic region. We may also say that the Arnold tongue is confined by the condition of the collision between the periodic attractor and the hole.

Using (30)–(34), we shall calculate the boundary conditions of period-one, -two, and -three regions. The results are shown in Figs. 5 and 8 with a fixed value of $A = 0.6$.

When $p = 1$ the image of the only periodic point t_{2mj} should always be itself and thus never be t_{mi}. The collision condition does not exist. Therefore the boundary condition should be solved by (31) and (32). In this case $g(t_{2mj}) = f_2(t_{2mj}) - 1 - t_{2mj}$. From (31) and (32) we get

$$\frac{I_i(1-A)}{I_i-(1-A)} < I_d < \frac{I_i(1+A)}{I_i-(1+A)} \quad \text{when} \quad I_i > 4A, \tag{35}$$

$$\frac{I_i(1-A)}{I_i-(1-A)} < I_d < \frac{I_i^2+2I_i(1-A)}{I_i-2(1-A)} \quad \text{when} \quad I_i < 4A, \tag{36}$$

They confine a period-one region between the lower line PB_1 (AB) and the upper line PB_1 $(EJ-JG)$ in Figs. 5 and 8.

When $p = 2$ we cannot exclude the collision condition and we have to consider whether holes can exist. By Eq. (27) we can express the condition of the appearance of the first-order hole as

$$f(t_{me}) < t_{mi} < f(t_{mm}). \tag{37}$$

The solution is

$$\frac{2I_i(1-A)}{I_i-2(1-A)} < I_d < \frac{2I_i(1+A)}{I_i-2(1-A)}, \tag{38}$$

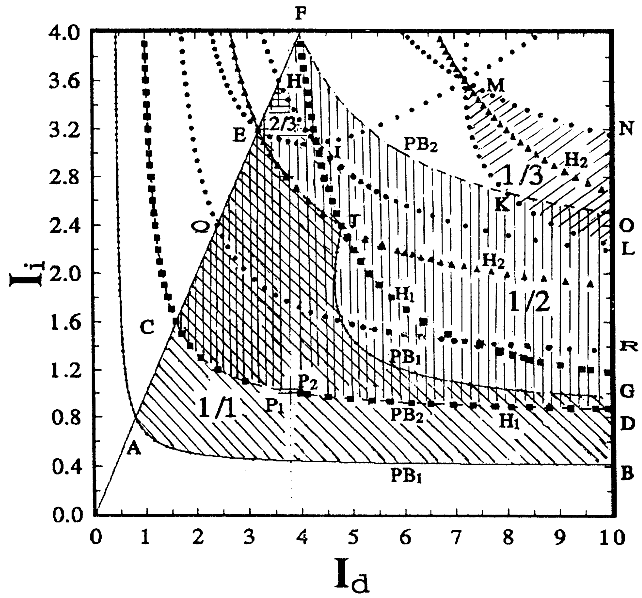

FIG. 8. Phase diagram to show the analytic results of several Arnold tongues and the corresponding regions where these periodic attractors coexist. The area covered by oblique lines at the lower part is the Arnold tongue $\frac{1}{1}$. The area covered by vertical lines is the $\frac{1}{2}$ tongue. The oblique lines at upper part cover the area $\frac{1}{3}$ and the horizontal lines cover $\frac{2}{3}$. The region between lines QR and MN is the possible stability range of the attractor with $W = \frac{1}{3}$ and the region between lines QR and HI is that of the attractor with $W = \frac{2}{3}$. The two lower boundaries coinciding along QR is occasional due to the chosen $A = 0.6$. All other lines in the figure have been explained in the text.

which confines a region between the two H_1 lines in Fig. 8. Also, the second-order hole's region has been solved by

$$f(t_{me}) < f^{-1}(t_{mi}) < f(t_{mm}). \tag{39}$$

This region is between the two H_2 lines in Fig. 8 and is expressed by

$$\frac{4I_i(1-A)}{I_i - 4(1-A)} < I_d < \frac{4I_i}{I_i - 4(1-A)}. \tag{40}$$

One can see there are no holes in the region beneath the lower line H_1.

In this case ($p = 2$) $g(t_{2mj})$ has two possible forms: $f_1(f_2(t_{2mj})) - 1 - t_{2mj}$ and $f_3(f_2(t_{2mj})) - 1 - t_{2mj}$. In the region

$$I_d < \frac{2I_i(1-A)}{I_i - 2(1-A)}, \tag{41}$$

i.e., below the lower H_1, the boundary of the period-two region should be solved by (31), (32), and (41). However, we find that they have no solution for the chosen parameter ($A = 0.6$) with both of the $g(t_{2mj})$ forms. While in the region between the two H_1, there is a hole and thus a $f_2^{-1}(t_{mi})$ on f_2. We should consider either $S_1 = (t_{mm}, f_2^{-1}(t_{mi}))$ or $S_2 = (f_2^{-1}(t_{mi}), t_{me})$ and then solve the boundaries of period-two tongue by (33), (34), and the first-order hole condition (38). The only solution, with $A = 0.6$, confines the region between the two H_1 lines, which are expressed by (38). In the region

$$I_d > \frac{2I_i(1+A)}{I_i - 2(1-A)}, \tag{42}$$

i.e., beyond the upper H_1, the boundary of the period-two region again should be solved by (31), (32), and (42). The second-order hole may appear here, however, it does not influence the period-two attractor, as discussed in Sec. VI. The solution is

$$\frac{2I_i}{I_i - 2} > I_d > \frac{2I_i(1+A)}{I_i - 2(1-A)} \quad \text{when} \quad I_i > 4A, \tag{43}$$

$$\frac{I_i^2 + 4I_i(1-A)}{I_i - 4(1-A)} > I_d > \frac{2I_i(1+A)}{I_i - 2(1-A)} \quad \text{when } I_i < 4A. \tag{44}$$

They confine a region between the upper H_1 and the upper line PB_2 (line FO) in Fig. 8. Putting the results together, we get the period-two region between both PB_2 lines (the lower PB_2 is superposed on lower H_1). It is expressed by

$$\frac{2I_i}{I_i - 2} > I_d > \frac{2I_i(1-A)}{I_i - 2(1-A)} \quad \text{when} \quad I_i > 4A, \tag{45}$$

$$\frac{I_i^2 + 4I_i(1-A)}{I_i - 4(1-A)} > I_d > \frac{2I_i(1-A)}{I_i - 2(1-A)} \quad \text{when } I_i < 4A. \tag{46}$$

There is an overlapping region of period-one and period-two Arnold tongues between the lower PB_2 and the upper PB_1 in Fig. 8. In this region the two periodic attractors with the rotation number $\frac{1}{1}$ or $\frac{1}{2}$ coexist. Following a vertical line in Fig. 8, one finds that the coexistence of the two attractors is created by the appearance of the first-order hole at lower H_1 and is destroyed by the vanishing of the period-one condition at upper PB_1.

When $p = 3$ we have to consider two cases where the rotation number $W = \frac{Q}{p}$ equals, respectively, $\frac{1}{3}$ or $\frac{2}{3}$. If $Q = 1$, $g(t_{2mj})$ has eight possible forms, where the term of f^{p-1} in Eq. (30) may be expressed as f_3f_3, f_3f_1, f_1f_3, f_1f_1, f_1f_2, f_2f_1, f_3f_2, and f_2f_3. As previously done, we must discuss all the cases. For the f_3f_3 form, we have a solution that confines a region between lines ML and MN in Figs. 8 and 5. Here line ML indicates the collision of the second-order hole with the periodic point on f_2 and line MN indicates the range of the stability of the $\frac{1}{3}$ tongue. The region can be expressed as

$$\frac{I_i(3-A)}{I_i-(3-A)} > I_d > \frac{I_i^2+2(1-A)I_i+\sqrt{I_i^4+36(1-A)^2I_i^2-4(1-A)I_i^3}}{2[I_i-4(1-A)]}. \tag{47}$$

For all the other forms of the term of f^{p-1}, i.e., f_3f_1, f_1f_3, f_1f_1, f_1f_2, f_2f_1, f_3f_2, and f_2f_3, our calculation shows that there is no solution in the range of chosen parameters.

If $Q=2$, $g(t_{2mj})$ also has the same eight possible forms. Similarly we have discussed all the cases and found that only for the form f_3f_1 the solution confines a region in Fig. 8. The region can be expressed as

$$\frac{I_i(3+A)}{I_i-(3+A)} > I_d > \frac{3I_i^2-2(1-A)I_i-\sqrt{9I_i^4+4(3-A)^2I_i^2-4(7+3A)I_i^3}}{2[I_i-2(1-A)]}, \tag{48}$$

which is the area between line EI and line HI in Figs. 8 and 5. Line EI indicates the collision of the second-order hole with the periodic point on f_2 and line HI indicates the range of the stability of the $\frac{2}{3}$ tongue.

One can see again two regions in Fig. 8 where period-two and period-three attractors coexist. The Arnold tongues $\frac{1}{3}$ and $\frac{1}{2}$ overlap in the region between line KL and upper PB_2, while the tongues $\frac{2}{3}$ and $\frac{1}{2}$ overlap in the region between lines EI and HI. This is all the $\frac{2}{3}$ region.

These analytical results have been compared with the numerical ones. The boundaries obtained from both methods are in very good agreement.

VI. DISCUSSION

In this section we discuss some questions that may be induced by the above analytical results. First, we discuss the specificity of the kind of coexistence of periodic attractors appearing in a both discontinuous and noninvertible map such as the present one [14,15].

The parameters of Figs. 7(a) and 7(b) are chosen at point P_1, just below the lower H_1 line in Fig. 8. One sees that there is no hole. The only attractor is the stable fixed point at S_1. When I_i increases a little bit to cross line H_1 and reaches P_2, a hole appears in the two-fold iterated map, as shown in Figs. 7(c) and 7(d). In Fig. 7(d) we can see three intersections between the $f^2(t)$ mapping function and the diagonal line, i.e., three stable fixed points of $f^2(t)$ marked by S_1, S_2, and S_2'. Each of them has its own basin of attraction. Referring to Fig. 7(c), we recognize that S_1 is the original period-one attractor. The hole region $(f_2^{-1}(t_{mi}), f_3^{-1}(t_{mi}))$ and the region of its first inverted image $(f_3^{-1}(f_2^{-1}(t_{mi})), t_{mi})$, i.e., the set of holes (this term has been defined in Sec. IV), becomes a loophole of its basin. These regions therefore form a basin of another attractor. Since the period-two condition exists here as shown in Figs. 8 and 5, it is reasonable to conclude that the period-two attractor occupies this new basin as shown in Fig. 7(d). Obviously, the coexisting period-two attractor appears and the old basin of the period-one attractor splits exactly when the hole appears. That is why we call it "hole-induced coexistence of attractors" [14,15]. In generic cases there may be many holes in an $f^p(t)$ map. If one of the coexisting attractors visits a hole formed by the multivalues of $f^{-k}(t_{mi})$ $(k<p)$, it will also visit all the $f_i^{-j}(t_{mi})$ $(k<j<p)$, the set of holes formed by the backward iterations of $f^{-k}(t_{mi})$, as we have discussed in Sec. IV, while another coexisting attractor always stays outside this set of holes. We thus denote this hole set by "principal set." In the example discussed here and in Sec. IV, the further inverted images of the hole fall in the forbidden region, as shown in Fig. 7(c), and thus do not exist. Therefore the basin of the attractor inside the principal set is only the first hole and its first backward image. In generic cases this basin should be the set of all the backward iterations of the first hole [14,15].

When P, the period of the Arnold tongues, increases, the number of holes that may appear in the P-fold iterated map also increases, as pointed out in Sec. IV. We then have to divide the characteristic region into more and more subregions in order to discuss the boundaries of the tongues. Furthermore, the hole-induced coexistence of periodic attractors have more chances to occur. What is the influence of these two new features on the Devil's staircase, if it still exists? This is the second question we discuss here.

In order to get an understanding of this question in a numerical way, we have computed some Devil's staircases. All the numerical results are in very good agreement with our analytical conclusions expressed in Figs. 5 and 8. Figures 9(a) and 9(b) show two of them. It is reasonable to say that there are still good Devil's staircases if we consider the fact that the current map is a model of a practical system with two competing frequencies. However, the Devil's staircases have two characteristics different from the ones in an everywhere differentiable map. The first is that the overlap of the neighboring steps are very common if the staircase is computed with different initial values as we have done here. According to the previous discussion, we have computed every step with only two initial values. One is always inside the principal set of holes and another is always outside it. The computational results are then put into the same figure and show the overlapping of the phase-locked steps in wide ranges. However, it should be noted that not every pair of neighboring steps is overlapping. In Figs. 9(a) and 9(b) one sees there may be an infinite number of small steps revealing the self-similar structure between the neighboring steps, which are not overlapping, as shown in the lower left inset of Fig. 9(a) and the upper right inset of Fig. 9(b). Furthermore, it seems that the overlap of neighboring steps erases all the middle steps and makes the staircase, in this part, very simple. The second characteristic of the staircases is that some steps, which are computed with the same rotation number W (P is quite large) but from different initial values, separated from each other as seen in the lower left inset of Fig. 9(a) and the upper right inset of Fig. 9(b). We argue that this is due to the fact that the number of subregions S_i is now large and that the jumping behavior at their edges may be very complicated. We may also add a third new characteristic, which is that the complete covering of S_h

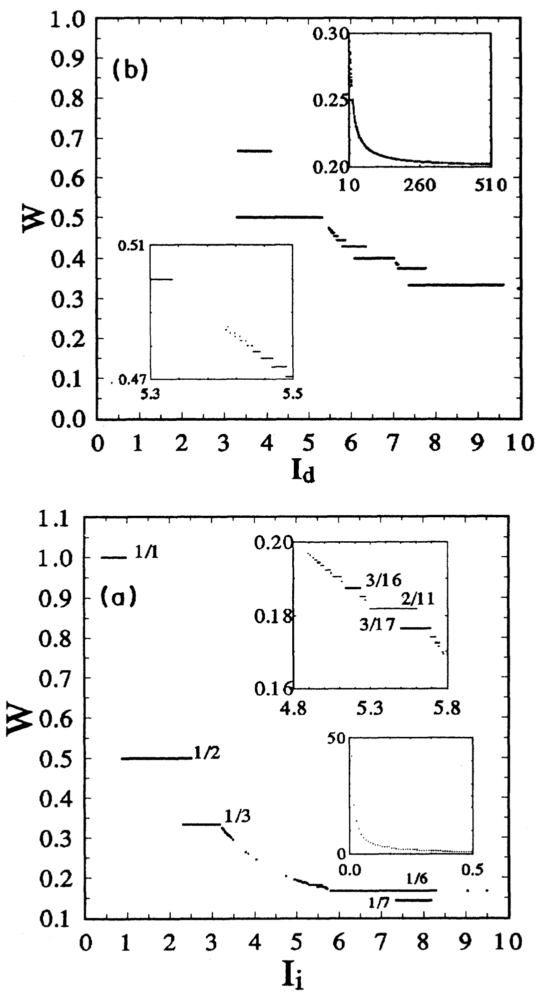

FIG. 9. (a) Devil's staircase computed at $A = 0.6$ and $I_i = 3.2$. The initial values were chosen, respectively, outside and then inside the principal set of holes. The first 400 iterations were dropped to avoid the transience. The left lower inset is the magnification of the related parts to show the self-similar structure. The right upper inset shows that W decreases monotonically when I_d increases. (b) Devil's staircase computed at $A = 0.6$ and $I_d = 9.5$ similarly. The upper inset is the magnification of the related parts to show the self-similar structure. The lower inset shows that W decreases monotonically when I_i increases. Please note that if $I_i > 9.5$, the system enters the chaotic region (see Fig. 5).

will also erase some steps, as can be seen in the region $I_i = 3.5 - 4.8$ in Fig. 9(b) (please refer to Fig. 5).

The third question one may ask is, How many holes are there in a P-fold iterated map describing a P-period attractor? We have to say that the answer is strongly dependent on the parameters and that it is quite difficult to calculate or even compute generally the number of the holes when P is large enough. In Fig. 10 we show a numerical result of hole numbers computed with the same parameters as in Fig. 9(a). The initial value is chosen inside the principal set of holes so that there is only one number of P for each I_d value. These numbers of P are addressed in Fig. 10. We can see that there are also some horizontal plateaus corresponding to different P values in this figure. Usually each P value corresponds to several plateaus. The number of holes, generally speaking, increases when P becomes larger. However, the rule is very complicated, as can be seen in Fig. 10. Also, the number of holes is not as large as we expected when P becomes larger. The reason is that the inverted images of the gap G as well as the extrema often fall in G and thus the increasing of the hole number is stopped as we have mentioned in Sec. IV.

The next question we discuss here is, What happens if there is a piece of mapping function with a slope tending to infinite instead of the gap so that the map becomes continuous? In order to answer this question, let us now return to map (1), which was introduced in Sec. II and described the trapezoidal wave-modulated relaxation oscillator. It is easy to see that the dynamics of this system in the supercritical region, where both slopes I_i and I_d of the relaxation are smaller than $\frac{A}{d}$, is qualitatively the same as we described above. That is because, in this region, map (1) is also composed of three linear branches,

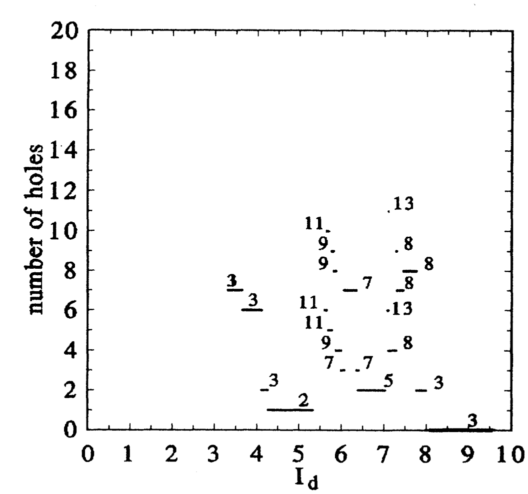

FIG. 10. Diagram computed with the same parameters as in Fig. 9(a) to show the number of holes appearing in the P-fold iterated mapping. The initial value was chosen inside the principal set of holes so that there is only one value of P for each I_d. The first 400 iterations were dropped to avoid the transience to determine P. All the P values are addressed with the numbers inside.

two of them having a slope of 1. Branch f_1 disappears when I_i becomes smaller and crosses the value $\frac{A}{d}$. Now, if we increase I_i from a value in this supercritical region to cross $\frac{A}{d}$, the f_1 branch will appear again and the discontinuity will disappear. The covered regions, holes, and all other features we discussed will also disappear. At the criticality, where $I_i = \frac{A}{d}$, the situation is exactly like what happened in the current question. We can say now that we are in a critical condition of a continuous phase transition. There are several scaling exponents signifying the criticality as several people have already discussed [35,28,31,17,11].

In this paper we have discussed the role of discontinuity, especially the interaction between discontinuity and noninvertibility, and the influence of this interaction on the system's dynamic behavior. We have shown that in a kind of one-dimensional map an interesting feature, namely, a hole, is convenient for explaining the mechanisms of some specific phenomena. Since the concept of hole denotes only a special pair of discontinuities, we may explain all the mechanisms of the dynamic phenomena by using only discontinuity. For example, we may express one of the boundary conditions of the Arnold tongues in the current system in the following ways: (i) It indicates that a periodic attractor vanishes via a collision with a hole and (ii) it indicates that whenever a discontinuity approaches the diagonal, a periodic orbit will vanish abruptly. There should be some specific phenomena whose mechanisms connect only with the concept of discontinuity and cannot be explained by a hole. One phenomenon discussed in this paper, namely, the covering of noninvertible region by gap images, serves as an example. Also, whenever a discontinuity approaches a chaotic attractor, the attractor will probably exhibit a sudden, topological change via different kinds of interior crises, as we have observed in the current system. We will report that the mechanism of one kind of the crisis can be explained by either discontinuity or a hole, but the mechanism of another kind can be explained only by discontinuity [36]. Therefore, the last question is, Can we obtain a more general, but still quantitative description for the mechanisms of all the specific dynamic phenomena in both discontinuous and noninvertible maps? We shall try to present a further study on this question in a future paper.

ACKNOWLEDGMENTS

The authors thank Professor Gu Yan for his helpful discussion. We also thank Dr. J. Martin for a careful reading of the manuscript. D.-R.H. wants to express his gratitude to Professor W. Martienssen at the University of Frankfurt for his hospitality and cooperation when these research topics were created and would also like to thank Dr. B. Christiansen for always interesting discussion in past years, especially for his important suggestions about the hole. The work was supported by the Chinese National Science Foundation and the Shaanxi Science Foundation. One of us (B.-H.W.) was supported by the Chinese National Basic Research Project "Nonlinear Science."

[1] J.P. Keener, Trans. Am. Math. Soc. **261**, 589 (1980).
[2] E.J. Ding and P.C. Hemmer, J. Stat. Phys. **46**, 99 (1987).
[3] P.C. Bressloff and J. Stark, Phys. Lett. A **150**, 187 (1990).
[4] M.C. de S. Vieira, E. Lazo, and C. Tsallis, Phys. Rev. A **35**, 945 (1987).
[5] C. Marriot and C. Delisle, Physica D **36**, 198 (1989).
[6] W.-M. Zheng and L.-S. Lu, Commun. Theor. Phys. **15**, 161 (1991).
[7] A.V. Holden and Y. Fan, Chaos, Solitons Fractals **2**, 349 (1992); **2**, 583 (1992).
[8] G.A. Petrillo and L. Glass, Am. J. Physiol. **246**, R311 (1984); M. Courtemanche, L. Glass, M.D. Rosengarten, and A.L. Goldberger, *ibid.* **257**, H693 (1989).
[9] L. Glass, Chaos **1**, 13 (1991); in *Directions in Chaos*, edited by B.-L. Hao (World Scientific, Singapore, 1987), Vol. 2, p. 90.
[10] B. Christiansen, P. Alstrøm, and M.T. Levinsen, Phys. Rev. A **42**, 1891 (1990).
[11] S. Habip, M. Bauer, D.-R. He, and W. Martienssen, Physica D **59**, 378 (1992).
[12] B. Christiansen, D.-R. He, S. Habip, M. Bauer, U. Krueger and W. Martienssen, Phys. Rev. A **45**, 8450 (1992).
[13] E. Catsigeras and R. Budelli, Physica D **56**, 235 (1992).
[14] D.-R. He, E.J. Ding, M. Bauer, S. Habip, U. Krueger, W. Martienssen, and B. Christiansen, Europhys. Lett. **26**, 165 (1994).
[15] D.-R. He, B.-H. Wang, M. Bauer, U. Krueger, W. Martienssen, and B. Christiansen, Physica D **79**, 335 (1994).
[16] K. Yagisawa, T. Kambara, and M. Naito, Phys. Rev. E **49**, 1320 (1994).
[17] D.-R. He, D. Wang, K.-J. Shi, C. Yang, L. Chao, and J. Zhang, Phys. Lett. A **136**, 363 (1989).
[18] H.E. Nusse, E. Ott, and J.A. Yorke, Phys. Rev. E **49**, 1073 (1994).
[19] H.E. Nusse and J.A. Yorke, Physica D **57**, 39 (1992).
[20] M. Bauer, S. Habip, D.-R. He, and W. Martienssen, Phys. Rev. Lett. **68**, 1625 (1992).
[21] D.-R. He, M. Bauer, S. Habip, U. Krueger, W. Martienssen, B. Christiansen, and B.-H. Wang, Phys. Lett. A **171**, 61 (1992).
[22] J. Fan, F. Ji, S. Guan, B.-H. Wang, and D.-R. He, Phys. Lett. A **182**, 232 (1993).
[23] J. Fan, F. Ji, B.-H. Wang, and D.-R. He, Phys. Lett. A **191**, 139 (1994).
[24] S. Wu, E.J. Ding, and D.-R. He, Phys. Lett. A **197**, 287 (1995).
[25] F. Ji and D.-R. He, Phys. Lett. A **177**, 125 (1993).
[26] C. Wunderlich, L. Moorman, and P.M. Koch, Phys. Lett. A **176**, 317 (1993).
[27] R. Richter, A. Kittel, K. Pyragas, J. Peinke, and J. Parisi,

Z. Phys. B **91**, 527 (1993).
[28] M.H. Jensen, P. Bak, and T. Bohr, Phys. Rev. A **30**, 1960 (1984); **30**, 1970 (1984).
[29] L. Glass and R. Perez, Phys. Lett. **90A**, 441 (1982); Phys. Rev. Lett. **48**, 1772 (1982).
[30] K. Kaneko, in *The Theory of Dynamical Systems and its Applications to Nonlinear Problems*, edited by H. Kawakami (World Scientific, Singapore, 1984).
[31] P. Alstrøm and M.T. Levinsen, Phys. Lett. A **128**, 187 (1988); P. Alstrøm, B. Christiansen, and M.T. Levinsen, Phys. Rev. Lett. **61**, 1679 (1988); Phys. Rev. A **40**, 7239 (1989); Phys. Rev. B **41**, 1308 (1990).
[32] K. Yagisawa, T. Kambara, and M. Naito (unpublished).
[33] P. Alstrøm, B. Christiansen, and M.T. Levinsen (private communication).
[34] S.-X. Qu, Y. Zhu, J. Fan, and D.-R. He (unpublished).
[35] P. Bak, in *Directions in Chaos* (Ref. [9]), Vol. 1.
[36] X. Ji, S. Guan, J. Sun, S.-X. Qu, and D.-R. He (unpublished).